A method to measure sound transmission via the malleus-incus complex

Dobrev, Ivo ; Ihrle, Sebastian ; Röösli, Christof ; Gerig, Rahel ; Eiber, Albrecht ; Huber, Alexander M ; Sim, Jae Hoon

Abstract: BACKGROUND: The malleus-incus complex (MIC) plays a crucial role in the hearing process as it transforms and transmits acoustically-induced motion of the tympanic membrane, through the stapes, into the inner-ear. However, the transfer function of the MIC under physiologically-relevant acoustic stimulation is still under debate, especially due to insufficient quantitative data of the vibrational behavior of the MIC. This study focuses on the investigation of the sound transformation through the MIC, based on measurements of three-dimensional motions of the malleus and incus with a full six degrees of freedom (6 DOF). METHODS: The motion of the MIC was measured in two cadaveric human temporal bones with intact middle-ear structures excited via a loudspeaker embedded in an artificial ear canal, in the frequency range of 0.5-5 kHz. Three-dimensional (3D) shapes of the middle-ear ossicles were obtained by sequent micro-CT imaging, and an intrinsic frame based on the middle-ear anatomy was defined. All data were registered into the intrinsic frame, and rigid body motions of the malleus and incus were calculated with full six degrees of freedom. Then, the transfer function of the MIC, defined as velocity of the incus lenticular process relative to velocity of the malleus umbo, was obtained and analyzed. RESULTS: Based on the transfer function of the MIC, the motion of the lenticularis relative to the umbo reduces with frequency, particularly in the 2-5 kHz range. Analysis of the individual motion components of the transfer function indicates a predominant medial-lateral component at frequencies below 1 kHz, with low but considerable anterior-posterior and superior-inferior components that become prominent in the 2-5 kHz range. CONCLUSION: The transfer function of the human MIC, based on motion of the umbo and lenticularis, has been visualized and analyzed. While the magnitude of the transfer function decreases with frequency, its spatio-temporal complexity increases significantly.

DOI: https://doi.org/10.1016/j.heares.2015.10.016

research, 340:89-98.
DOI: https://doi.org/10.1016/j.heares.2015.10.016

Accepted Manuscript

A method to measure sound transmission via the malleus-incus complex

Ivo Dovrev, Sebastian Ihrle, Christof Röösli, Rahel Gerig, Albrecht Eiber, Alexander M. Huber, Jae Hoon Sim

PII: S0378-5955(15)30095-2

DOI: 10.1016/j.heares.2015.10.016

Reference: HEARES 7043

To appear in: *Hearing Research*

Received Date: 31 July 2015

Revised Date: 22 October 2015

Accepted Date: 29 October 2015

Please cite this article as: Dovrev, I., Ihrle, S., Röösli, C., Gerig, R., Eiber, A., Huber, A.M, Sim, J.H., A method to measure sound transmission via the malleus-incus complex, *Hearing Research* (2015), doi: 10.1016/j.heares.2015.10.016.

A method to measure sound transmission via the malleus-incus complex

Ivo Dovrev[1,*], Sebastian Ihrle[2], Christof Röösli[1], Rahel Gerig[1], Albrecht Eiber[2], Alexander M Huber[1], Jae Hoon Sim[1]

[1]University Hospital Zurich, University of Zurich, Zurich, Switzerland

[2]University of Stuttgart, Stuttgart, Germany

[*]Corresponding author: Otolaryngology, Head and Neck Surgery, University Hospital Zurich, University of Zurich, Frauenklinikstrasse 24, 8091 Zurich, Switzerland; ivo.dobrev@uzh.ch

For submission to Hearing Research as part of the proceedings of the MEMRO 2015 meeting, Aalborg, Denmark, July 1–5, 2015

Abstract

Background: The malleus-incus complex (MIC) plays a crucial role in the hearing process as it transforms and transmits acoustically-induced motion of the tympanic membrane, through the stapes, into the inner-ear. However, the transfer function of the MIC under physiologically-relevant acoustic stimulation is still under debate, especially due to insufficient quantitative data of the vibrational behavior of the MIC. This study focuses on the investigation of the sound transformation through the MIC, based on measurements of three-dimensional motions of the malleus and incus with a full six degrees of freedom (6 DOF).

Methods: The motion of the MIC was measured in two cadaveric human temporal bones with intact middle-ear structures excited via a loud speaker embedded in an artificial ear canal, in the frequency range of 0.5-5 kHz. Three-dimensional (3D) shapes of the middle-ear ossicles were obtained by sequent micro-CT imaging, and an intrinsic frame based on the middle-ear anatomy was defined. All data were registered into the intrinsic frame, and rigid body motions of the malleus and incus were calculated with full six degrees of freedom. Then, the transfer function of the MIC, defined as velocity of the incus lenticular process relative to velocity of the malleus umbo, was obtained and analyzed.

Results: Based on the transfer function of the MIC, the motion of the lenticularis relative to the umbo reduces with frequency, particularly in the 2-5 kHz range. Analysis of the individual motion components of the transfer function indicates a predominant medial-lateral component at frequencies below 1 kHz, with low but considerable anterior-posterior and superior-inferior components that become prominent in the 2-5 kHz range.

Conclusion: The transfer function of the human MIC, based on motion of the umbo and lenticularis, has been visualized and analyzed. While the magnitude of the transfer function decreases with frequency, its spatio-temporal complexity increases significantly.

Keywords: Malleus-Incus complex, 3D Laser Doppler Vibrometer, rigid-body motion, human middle-ear, 3D transfer function, incudo-malleolar joint; micro-CT

Abbreviations: ASTM - American Society for Testing and Materials; DOF - degree(s) of freedom; IMJ - incudo-malleolar joint; ISJ - incudo-stapedial joint; LDV - laser Doppler vibrometry; LPI - lenticular process of the incus; MIC - malleus-incus complex; RBM - rigid body motion; SNR - signal-to-noise ratio; TB - temporal bone; 3D - three dimensional

1. Introduction

Acoustically-induced motions of the tympanic membrane cause three-dimensional vibrations of the middle-ear ossicles. Sophisticated techniques are needed to measure the vibrational motions of the middle-ear ossicles because the amplitude of the ossicular vibration is on a nanometer scale. Previous investigations (Decraemer et al. 1999; Puria 2003) have revealed that the Laser Doppler Vibrometer (LDV) provides sufficiently sensitive, reliable and accurate measurements for determining vibration modes of the middle-ear bones.

Considering motion of each of the middle-ear ossicles (i.e., the malleus, incus, and stapes) as a rigid body motion under physiologically-relevant acoustical stimulation, three-dimensional (3D) motions of each ossicle have six degrees of freedom (DOF), consisting of three translations and three rotations, and thereby the ossicular motion of the middle-ear bones can be described in a common reference frame. From a theory of classical dynamics, the six rigid-body motion (RBM) components can be determined when the spatial motion components and coordinates of more than three non-co-linear points on the rigid body are known. Decraemer et al. (1994) presented a method for determining three translational components at a specific point on the middle-ear bones from measurements using a one-dimensional (1D) LDV. They mounted temporal bones on two stacked goniometers and measured velocities using a laser Doppler vibrometer from several different angles, which were provided by rotations of the two goniometers. Recent developments and commercialization of 3D LDV systems with three built-in laser beams, oriented at three independent measurement angles, allow for accurate and simultaneous measurements of all three translational components at a measurement point.

In the previous studies, spatial motion of the stapes was measured for humans (Hato et al. 2003; Sim et al. 2010a) and for guinea pigs (Sim et al. 2010b) with an assumption that in-plane motion of the stapes along the footplate plane is restricted due to anatomy of the annular ligaments, and thus motion of the stapes has only three dominant spatial motion components. Lauxmann et al. (2012) measured motion of the human stapes with the full six DOF, but in their measurements the cochlea was drained, which may have significantly changed the physiological response of the samples. They measured 3-D motion components at nine points on the medial side of the footplate using a 3-D LDV system, and reconstructed the six rigid-body motion components from the measurement. Decraemer et al. (2007) also measured motion of the gerbil stapes with the full six degrees of freedom. In their study, the measurement points were aligned at the center of the rotations of the goniometers, and thus

the location of the measured points could be maintained during the rotations by the goniometers.

While spatial motion of the stapes has been measured in several previous studies, measurements of spatial motion of the malleus or the incus have involved technical difficulties. First, the spatial motions of each of the malleus and incus are expected to have full six degrees of freedom involving their relative motion at the incudo-malleal joint (IMJ), and thus simplification of the spatial motion is not applicable. Second, surgical opening for access to the malleus and incus is limited because the malleus-incus complex is suspended by several ligaments and tendons and those must not be damaged to measure physiological motion of the malleus-incus complex. Such difficulty in surgical opening becomes more serious with the 3D LDV system because access of the three beams from the 3D LDV system requires wider surgical opening. Sim et al. (2004) measured spatial motion of the malleus-incus complex with full six degrees of freedom, but in their measurements, the malleus-incus complex was isolated, with the stapes and extraneous bones removed, to obtain sufficient access of the laser beam of the LDV system to the malleus and the incus. This study found significant relevant motion between the malleus and incus that increased with frequency. Decraemer et al. (2014) measured the spatial motion of the MIC in living gerbils and found a frequency dependence on the direction of the instantaneous rotational axis (hinged motion) between the malleus and incus. In this study they removed circular pars flaccida for access the LDV laser beam. In addition, in their measurements, sophisticated measurement setup and procedures with a custom-made positioning system were needed with use of a 1D LDV system.

In this study, a method to measure and determine spatial motions of the malleus and the incus with the full six DOF using a 3D LDV system is introduced, and the method is applied to two human cadaveric temporal bones. The 3D LDV system is positioned by several different angles with respect to the specimen due to limited access of the laser beam to the malleus and the incus. To identify spatial coordinates of the measurement points on the ossicles with different orientations of the 3D LDV system, spatial registration techniques using micro-CT imaging are used.

2. Methods

2.1. Temporal Bone Preparation

A fresh cadaveric temporal bone (TB), TB1, and a frozen TB, TB2, were used for this study. The fresh TB was harvested within 24 hours after death and was preserved in thiomersal 0.1 % ($C_9H_9HgNaO_2S$) solution at 4° C. The frozen TB was also harvested within 24 hours after death and was frozen immediately. The use of human TBs in this study was approved by the Ethical Committee of Zurich (KEK-ZH-Nr. 2012-0007).

A canal-wall-up mastoidectomy including posterior tympanotomy and a wide epitympanectomy were performed subsequently to expose the malleus-incus complex as much as possible. After the surgical opening, the superior part of the malleus head and incus body, the manubrium of the malleus, and the long process of the incus were exposed. The intact tympanic membrane (TM) was confirmed by microscopic view, and all suspensory attachments to the middle-ear ossicles, which include ligaments and tendons, were left intact, during the preparation. The external ear canal was drilled down near the tympanic membrane for stable positioning of an artificial ear canal (AEC) without air leakage. The AEC allowed to for the control of the volume and distance between the microphone probe and the TM center, maintained at 5ml and approximately 5 mm, respectively. (Sim et al., 2010, 2012; Lauxmann et al., 2012; Gerig et al. 2015).

Several custom-made markers were glued on the peripheral bones as references for identification of the LDV measurement frame (see Section 2.3), and were held in position during the measurements. The marker consists of a silica glass tube (diameter of 0.3 mm and length of 1-3mm) and a copper wire (diameter of 0.05 mm) embedded in the silica glass tube.

2.2 Measurement of vibration of the malleus and incus

Figure 1 illustrates the measurement setup schematically. The major components of the setup are: 1) a three-dimensional Laser Doppler Vibrometry (3D LDV, CLV-3000, CLV-3D, Polytec, Germany) system for measurements of the motion of the ossicles; 2) speaker and microphone for application of controlled acoustic stimuli; 3) mechanical positioners for control of the relative position between the sample and the 3D LDV.

The TBs were mounted on a custom-made three-axis gimbal stage allowing for control over the viewing angle to the sample. The position of the 3D LDV was controlled via a 3-axis positioner consisting of three electrically-driven micro-positioning translation stages (PI Physik Instrumente M-126.CG1/DG1, Karlsruhe, Germany) mounted on a support frame. The position of the 3D LDV laser spot was identified by displacement encoders integrated into the

translational stages, with a bidirectional repeatability of 2.5 μm. The control of the translational stages and recording of the position of the 3D LDV system from the displacement encoders was done in real-time by dSPACE (Paderborn, Germany). A USB microscopic camera (Digimicro 1.3, DNT, Germany) was attached to the measurement head of the 3D LDV system by means of a reflective prism (mirror) for visual observation of the laser spot on the surface of the malleus and incus (Lauxmann et al. 2012).

A loudspeaker (ER-2, Etymotic Research, USA) and a microphone (ER-14C, Etymotic Research, USA) were placed in the AEC, in order to generate the sound stimuli and monitor the sound pressure levels inside the AEC. Two sets of multi-frequency harmonic signals (0.5-2 kHz and 2-5 kHz) were generated by a function generator embedded in the dSPACE data acquisition system and were delivered to the loudspeaker via an amplifier. To reduce the crest factor of the resulting signal and prevent the peak amplitude of the resulting signal from exceeding the maximum allowable voltage to the loudspeaker (2 Volts), the phases of the sinusoidal components were optimized using a Schroeder multi-sine phase distribution. (Gatto et al. 2010). The frequency steps were 12.5 Hz through the stimulation frequency range. With the two sets of the multi-frequency harmonic signals, AEC pressure levels of 80-95 dB SPL were obtained.

With the acoustic stimulation, spatial motion components (i.e., *XYZ* components) of each measurement point were measured by the 3D LDV system. The measured signals were digitized with a sampling frequency of 51.2 kHz after filtering with VBF 44 filter modules (Kemo, Dartford, United Kingdom) with the low-pass filter cut-off set at 12.5 kHz. The recording of the data was done through eight signal channels in dSPACE, which consists of six channels from the 3D-LDV unit (three raw signals and three Cartesian signals obtained from the build in geometry module), a channel for the pressure in the ear canal, and a channel for the excitation signal. The measurements at each point were repeated 30 times (30 measurement blocks), and were averaged. All the measurement procedures were controlled by an external computer using a custom-made algorithm.

The measurements of the vibrational motion were performed at 6-8 points on the malleus, and 8-10 points on the incus. The measurement points were located on the superior part of the malleus head and incus body, the manubrium of the malleus, and the long process of the incus, and access of the laser beams from the 3D LDV system could be obtained with several different orientations of the TBs (three orientations for TB1 and two orientations for TB2).

During the velocity measurement, *XY* coordinates of the measurement points in the 3D LDV measurement frame (*XYZ* coordinate system), in which the *Z*-axis along the laser beam (positive direction of the *Z*-axis toward the LDV head) and the *XY* plane is perpendicular to the laser beam, were recorded by the displacement encoders of the translational stages. The *XY* coordinates of one end of the markers in the 3D LDV measurement frame were also recorded. The recorded *XY* coordinates of the measurement points and markers were used for identification of the 3D LDV measurement frame and the measurement points (see Section 2.3).

2.3 Frame Registration

2.3.1 Micro-CT Imaging

After the velocity measurement, the TB with the markers (see Section 2.1 for details) was scanned by a high-resolution micro-CT scanner (vivaCT 40, SCANCO Medial AG, Switzerland). The resolution was set to 15 μm, and the photon energy level was set to 55 keV (Sim and Puria 2008). The 3-D volumes of the malleus, the incus, the stapes, and the markers were reconstructed from the micro-CT slice images. The copper wires in the markers were clearly visible and distinguishable from bones in the micro-CT images because the copper had much larger x-ray attenuation than the bones and soft tissues (Sim et al. 2009, 2012).

2.3.2 Intrinsic Frame (anatomical frame)

The *xyz* coordinate system of the intrinsic frame (i.e., anatomical frame) was defined based on the geometry of the medial surface of the stapes footplate (Sim et al. 2013) and the center of mass of the malleus-incus complex (Note that the *xyz* coordinate system is attributed to the intrinsic frame whereas the *XYZ* coordinate system is attributed to the LDV measurement frame). First, in order to determine the directions of the intrinsic frame axes, surface models of the stapes in STL (Standard Tessellation Language) format were obtained from micro-CT images. The surface models were imported into a commercial software, RapidForm XOS2 **(**3D Systems Corp., USA)**,** and a plane, which best fit to the medial surface of the footplate, was obtained. On the plane, the posterior-anterior direction along the long axis of the footplate was set as the *x*-direction, the inferior-superior direction along the short axis of the footplate as the *y*-direction, and the medial-lateral direction (i.e., the direction normal to the plane) as the *z*-direction. Using the right-hand rule for the right ear (TB1) and the left-hand rule for the left ear (TB2), the anterior, superior, and lateral directions were set as the positive *x*, *y*, and *z* directions. The directions of the long and short axes of the footplate

were determined such that the ratio of the length along the short axis to the length along the long axis was minimized (Sim et al. 2013).

While the *xyz* directions of the intrinsic frame were determined with surface models of the stapes, the center of mass of the malleus-incus complex, which was calculated from 3-D volume data of the malleus-incus complex, was set as the origin of the intrinsic frame. In the calculation, only the high-density bony parts were considered, and uniform density was assumed for the high-density parts (Sim et al. 2007, 2013).

2.3.2 Registration into intrinsic frame

Once the 3-D features of the middle-ear ossicles and the markers reconstructed from the micro-CT frame were registered into the intrinsic frame, transformation between the LDV measurement frames and the intrinsic frame (anatomical frame) was obtained, based on the coordinates of the markers in both frames. For the registration, the 3-D features of the middle-ear ossicles and the markers in the intrinsic frame were transformed to each of the LDV measurement frames by rotations and translations, such that the *XY* coordinates of the markers recorded in the LDV measurement frame (see Section 2.2) fit the location of the markers in the intrinsic frame. Thereby, transformation from the intrinsic frame to the LDV measurement frame was defined by the rotations and translations performed during the registration. Figure 2a illustrates the 3-D features of the middle-ear ossicles and the markers aligned into the LDV measurement frame for orientation of TB1.

Then, since only the *XY* coordinates of the measurement points were recorded in the LDV measurement frame, identification of the *Z* coordinates of the measurement points was required. The identification of the *Z* coordinates of the measurement points was done using a custom-made ray-tracing algorithm, which is based on the OPCODE collision detection library (Terdiman 2001) and implemented in Matlab (MathWorks, USA). For each measurement point, a virtual laser beam was made such that it passed through the *XY* coordinates of the measurement point. The virtual laser beam started at a point located on the side of the LDV unit with a positive *Z* coordinate larger than the maximum value of the surface geometry, and was pointed toward the surface geometry. Then, the coordinates of the first intersection point between the virtual laser beam and the surface geometry were the coordinates of the measurement point in the LDV measurement frame (right in Fig. 2b).

After the transformation from the intrinsic frame to the LDV measurement frame was identified including the *Z* coordinates of the measurement points in the LDV measurement frame, it was reversed to obtain the transformation of the measurement points from the LDV

measurement to the intrinsic frame. Figure 3 illustrates the measurement points in each of the three LDV measurement frames (i.e., three different orientations) and all the corresponding points registered in the intrinsic frame (TB1).

2.4. Calculation of the rigid body motion (RBM) components

Once all the measurement points on the malleus and the incus are registered to the intrinsic frame, the vector $\mathbf{v}_r$ of the six rigid-body motion components of each of the malleus and the incus is related to the velocity vector $\mathbf{v}_m$ at the point m on the bone in the intrinsic frame by

$$\mathbf{v}_m = \mathbf{B}_m \mathbf{v}_r , \tag{1}$$

with $\mathbf{B}_m = \begin{bmatrix} 1 & 0 & 0 & 0 & z_m & -y_m \\ 0 & 1 & 0 & -z_m & 0 & x_m \\ 0 & 0 & 1 & y_m & -x_m & 0 \end{bmatrix}$ and $\mathbf{v}_r = \begin{Bmatrix} \mathbf{v}_o \\ \boldsymbol{\omega} \end{Bmatrix} = \begin{Bmatrix} v_{ox} \\ v_{oy} \\ v_{oz} \\ \omega_x \\ \omega_y \\ \omega_z \end{Bmatrix}$.

where $\mathbf{v}_o$ and $\boldsymbol{\omega}$ indicates vectors for the translational velocity at the origin and the rotational velocity of the rigid body, and (x_m, y_m, z_m) are the coordinates of the point m in the intrinsic frame. The velocity vector $\mathbf{v}_m$ of the point m in the intrinsic frame is obtained from the corresponding velocity vector $(\mathbf{v}_m)_{\mathrm{MF}}$ in the LDV measurement frame by

$$\mathbf{v}_m = \mathbf{A}_{\mathbf{MF}\rightarrow\mathbf{IF},m} (\mathbf{v}_m)_{\mathbf{MF}} , \tag{2}$$

where $\mathbf{A}_{\mathbf{MF}\rightarrow\mathbf{IF},m}$ indicates transformation matrix from the LDV measurement frame to the intrinsic frame, which is obtained based on methods described in Section 2.3. Combining Eqs. (1) and (2),

$$(\mathbf{v}_m)_{\mathbf{MF}} = \mathbf{A}_{\mathbf{IF}\rightarrow\mathbf{MF},m} \mathbf{B}_m \mathbf{v}_r , \tag{3}$$

with $\mathrm{A}_{\mathrm{IF}\rightarrow\mathrm{MF},m} = \mathrm{A}_{\mathrm{MF}\rightarrow\mathrm{IF},m}^{-1}$ (transformation matrix from the intrinsic frame into the LDV measurement frame). Combining all n measurement points, Eq. (3) leads to

$$\mathbf{v}_{\mathbf{MF}} = \mathbf{C}\mathbf{v}_r , \tag{4}$$

with $\mathbf{v}_{\mathbf{MF}} = \begin{Bmatrix} (\mathbf{v}_1)_{\mathbf{MF}} \\ (\mathbf{v}_2)_{\mathbf{MF}} \\ \vdots \\ (\mathbf{v}_n)_{\mathbf{MF}} \end{Bmatrix}$ and $\mathrm{C} = \begin{Bmatrix} \mathrm{A}_{\mathrm{IF}\rightarrow\mathrm{MF},1}\mathrm{B}_1 \\ \mathrm{A}_{\mathrm{IF}\rightarrow\mathrm{MF},2}\mathrm{B}_2 \\ \vdots \\ \mathrm{A}_{\mathrm{IF}\rightarrow\mathrm{MF},n}\mathrm{B}_n \end{Bmatrix}$.

To determine the six rigid-body motion components, at least three non-collinear points are needed for each of the malleus and the incus (i.e., $n \geq 3$). Since the measurements of the vibrational motion were performed at 6-8 points on the malleus and 8-10 points on the incus, the vector $\mathbf{v}_r$ of the rigid-body motion components was calculated by the method of least squares error as

$$\mathbf{v}_r = \left(\mathbf{C}^{\mathrm{T}}\mathbf{C}\right)^{-1}\left(\mathbf{C}^{\mathrm{T}}\mathbf{v}_{\mathbf{MF}}\right). \quad (5)$$

2.5. Optimization of the RBM calculations

While Eq. (5) allows for an RBM fit based on the velocity data from all measurement points (i.e., 6-10 points on each ossicle), in practice, not all the measured data from all measurement points are suitable for the RBM calculation due to issues with poor signal-to-noise ratio (SNR) of the velocity data or ambiguities in the spatial location of the measurement points. In order to provide a deterministic approach to choosing an optimal data set by excluding problematic velocity data and points, we designed an automatic selection procedure that accounts for time waveform coherence, SNR, and RBM fit accuracy of measurement data.

The procedure consisted of two stages. In the first stage, the waveform of each measurement block was compared to the waveform of all other blocks. Based on this, only "good" blocks, defined as having less than 5% average deviation from the rest, were used for further processing. Then data were averaged among "good" blocks in the frequency domain, and the corresponding SNR was estimated by comparison with noise floor measurements. Velocity components with an average SNR of less than 10 dB were excluded from further calculations.

In the second stage of the automatic selection procedure, a diagram, which is shown in Fig. 4, the vector $\mathbf{v}_r$ of the six rigid-body motion components was calculated, the velocity vector $(\mathbf{v}_m)_{\mathrm{MF}}$ of each measurement point was reversely calculated from $\mathbf{v}_r$ using equation (3), and the results were compared with the originally measured velocity components. In the case that any reversely calculated velocity component showed a large difference from the corresponding measured velocity component, the velocity component was removed and the rigid-body motion components were recalculated. The iterations were stopped when the difference between the RBM fit and the measured data converged to < 3 dB, or when the maximum number of iterations (i.e., N < 10) was reached. For the final data set, the average ratio between the final RBM fit and measured data was 1-2 dB.

3. Results

3.1 Rigid-body motion (RBM) components of the malleus and the incus

Figure 5 represents the rigid body motion (RBM) components of the malleus (solid) and the incus (dashed), normalized by the ear canal pressure, for the fresh temporal bone (TB1, Fig. 5a) and frozen temporal bone (TB2, Fig 5b). The results from the two sets of harmonic signals showed continuity at the border frequency (i.e., at 2 kHz), for both magnitude and phase

Comparison between the translational components of the malleus at the center of mass of the malleus-incus complex (i.e., origin of the intrinsic frame) shows that, at frequencies below approximately 3.5 kHz, the v_{oy} (velocity component in superior direction) and v_{oz} (velocity component in the median direction) are larger than the v_{ox} (velocity component to the anterior direction), for both TBs. This can be explained by the hinged lever motion of the malleus (Bekesy 1960; Wever and Lawrence 1954), considering some amounts of offset of the center of mass of the malleus-incus complex from the rotational axis of the hinged motion. The rotational component ω_x (rotation about the posterior-anterior axis) of the malleus, which corresponds to the hinged motion, is larger than other rotational components at low frequencies (below 2.5 kHz for TB1 and below 4 kHz for TB2). The rotational component ω_y (rotation about the inferior-superior axis) of the malleus becomes relatively large at high frequencies.

In the translational components of the incus at the center of mass of the malleus-incus complex, the v_{oy} and v_{oz} have larger magnitudes than the v_{ox} at low frequencies (below 2.5 kHz for TB1 and below 1.2 kHz for TB2). The rotational component ω_x of the incus has larger magnitudes than other rotational components below 1.5 kHz, and all the rotational components have similar magnitudes at higher frequencies, for both TBs.

The malleus and the incus show differences in their RBM components for both TBs, indicating relative motion between the two ossicles. In TB1, the magnitudes and phases of v_{oy} and ω_x are similar in the whole frequency range and below 1.2 kHz, respectively. All other components showed differences in magnitude and phase. The TB2 also shows similar magnitudes and phases of ω_x up to 1.5 kHz. In TB2, the v_{oy} and ω_z have similar magnitudes and phases in the entire considered frequency range. In both TBs, the rotational component ω_y in the malleus has larger magnitudes than the corresponding component in the incus above 2.5 kHz.

3.2 Transfer function of the lenticularis relative to the umbo

Figure 6 illustrates velocities at the umbo of the malleus and at the lenticular process of the incus (LPI), normalized by the ear canal pressure, for the fresh temporal bone (TB1, Fig. 6a) and frozen temporal bone (TB2, Fig. 6b). The shaded areas in the figures indicate the normal ranges (95% confidence interval) of the umbo motion (left upper in Fig. 6a and Fig. 6b), based on measurements of in-vivo (Goode et al. 1996; Huber et al. 2001; Whittemore e t al. 2004) and temporal bones (Goode et al.1994; Kurokawa et al. 1995; Willi et al. 2002; Rosowski et al. 2004), and the stapes motion (right upper in Fig. 6a and Fig. 6b), based on the American Society for Testing and Materials (ASTM) standard (F2504-05, Philadelphia, 2005).

Both TBs indicate a predominant component in the medial-lateral direction (v_{uz} and v_{iz}) that is 5-15 dB higher at lower frequencies (i.e., < 2 kHz) than the other components. Considering the fact that the rotational component ω_x contributes mainly to the translational component of the medial-lateral direction at the umbo and the lenticular process, such results are consistent with observations from data in Fig. 5. At the lenticular process of TB1, the component in the medial-lateral direction still remains larger than other components at higher frequencies, but the differences were less than < 5 dB above 1.5 kHz. The phase was similar for the components in the *x* and *y* directions for the umbo of the malleus and the LPI in TB1. In TB2, all the three velocity components of the LPI have similar magnitudes above 2 kHz.

4. Discussion

4.1. Accuracy of the RBM fit

As described in the Introduction, difficulties in measuring three-dimensional motions of the malleus–incus complex are caused mainly by limitations in the surgical opening for access of the laser beams of the 3D LDV system to the malleus and the incus without damage to the suspensory attachments in the middle ear. Though the superior part of the malleus head and incus body, the manubrium of the malleus, and the long process of the incus were exposed by a combined surgical opening of a canal-wall-up mastoidectomy and an epitympanectomy, the measurements were performed with several different angular positions of the 3D LDV laser beams to obtain a sufficient number of the measurement points. With such approaches, identification of the angular positions of the 3D LDV laser beams and registration of the measurement points to the anatomical intrinsic frame were necessary. This study describes methodologies to resolve the problems and thus measure the full three-dimensional motions of the malleus and the incus.

In addition, in this study, an algorithm to exclude erroneous data and measurement points was used (see Section 2.5). In the first stage of the algorithm, data blocks with poor SNR or waveform conformity were excluded, resulting in the removal of < 5 (out of 30) blocks of the data, on average for all measurements. In the second stage of the algorithm, approximately 10-20% of the velocity components were excluded, and the RBM was recalculated with the remaining components. Figure 7 illustrates the magnitudes of the measured data (solid) in comparison with the magnitude of the corresponding components recalculated from the obtained RBM (dashed), for the measurement points on the incus in TB2. In this example, only the velocity components used for the final RBM calculation were shown in Fig. 7 (i.e., *X* component at I3, I4, and I7, and *Y* component at I5 and I9 were removed during the optimization procedures, as shown in Fig. 7). The recalculated components generally show good agreement with the originally measured components.

4.2. Relative motion at the incudo-malleolar joint

In Fig. 5, while a part of the RBM components, including the rotational component ω_x, have similar magnitudes, some RBM components show phase and magnitude differences between the malleus and the incus in specific frequency ranges. However, considering the fact that the rotational component ω_x, which corresponds to the hinged motion (rotation around the inferior-superior direction) of the malleus and incus, is larger than other rotational components at nearly all frequencies below 3-4 kHz, the malleus and the incus show smaller

relative motions below 1.2 kHz, larger relative motions in the 1.5 – 4.5 kHz range, and again reduced relative motion above 4.5 kHz. Another interesting observation was that the rotational component ω_y (rotation about the inferior-superior direction) in the malleus has larger magnitudes than the corresponding component in the incus at higher frequencies above 2.5 kHz. Such relatively large magnitudes of the malleus were predicted by Puria and Steele (2010), where the rotational motion of the malleus about the inferior-superior direction was described as a "twisting motion". From their observation of anatomy of the eardrum, malleus, and the incudo-malleal joint (IMJ), they predicted that the "twisting motion" would be large at high frequencies in large mammals such as human and cat, and the large "twisting motion" of the malleus would be transferred to the incus with reduced magnitudes via the mobile IMJ in the large mammals. Both components, ω_x and ω_y, show comparable magnitudes at high frequencies, indicating a complex combination of hinged and twisting motions.

The frozen bone (TB2) shows smaller relative motions between the malleus and the incus than the fresh bone (TB1), for all the RBM components, indicating lower mobility of the IMJ in the frozen temporal bone. However, only one fresh and one frozen temporal bones were used in this study, and more samples will be needed to confirm the possible difference between fresh and frozen conditions of the temporal bones. In addition, it has been known that there exist large amounts of individual variance in ossicular motion across samples. As shown in Fig. 6 (shaded areas), individual variance in the velocities at the umbo of the malleus and at the lenticular process of the incus can be as large as 15 dB through the frequency range considered in this study.

4.3. Transmission loss in the malleus-incus complex

Figure 8 illustrates the ratios of the velocity at the LPI to the velocity at the umbo, which are shown in Fig. 6, for the velocity component v_z (i.e., v_{iz}/v_{uz}). While the frozen and fresh temporal bones showed large differences in each of the umbo velocity and the LPI velocity (Fig. 6), the magnitude ratio and phase difference between the umbo velocity and the LPI velocity in z-direction were very similar for the bones of the two different conditions (within <3dB on average across frequencies). Since the LPI is in close proximity to the input of the incudo-stapedial joint (ISJ), and since previous studies (Huber et al. 2003; Peacock et al. 2015; Allan et al. 2013) indicate low relative motion across the ISJ, the LPI motion can be assumed to be representative of the motion of the stapes head. Based on that, the velocity component v_{iz} of the LPI can be considered as the piston-like motion of the stapes. In both TBs, the velocity component in the direction of the piston-like motion is attenuated, through

the malleus-incus complex, by less than 5 dB below 1.8 kHz, and by more than 10 dB above 2 kHz. The attenuation is explained by the observation that the incus has smaller magnitudes of the hinged rotational motion than the malleus at high frequencies (see the rotational component ω_x in Fig. 5). Assuming that the motion component v_{iz} at the lenticular process is representative of the piston-like motion of the stapes, previous works supports the attenuation at high frequencies.

As the reduction of the hinged rotational motion through the malleus and the incus is caused by the mobility of the IMJ, immobilization of the IMJ is supposed to increase sound transmission through the middle ear. In a study by Willi (2003), transmission through the malleus-incus complex could be increased at high frequencies above 3 kHz by immobilizing the IMJ. Offergeld et al. (2007) also demonstrated that the amplitude of the stapes motion is increased in the frequency range of 1.2-5 kHz with immobilization of the IMJ. Recently, Gerig et al. (2015) showed that the piston-like motion of the stapes with the immobilized IMJ is increased by 5-8 dB above 2 kHz compared to the corresponding motion with the mobile IMJ. The reason why the IMJ is mobile even with reduction of the middle-ear transmission has not been revealed.

Additionally, the relative phase difference between the umbo and LPI, with a maximum of 70deg at 2 kHz, suggests a frequency-dependent group delay of approximately 100μs, which is consistent with a middle-ear group delay of 134μs (including the tympanic membrane and ossicles) reported by O'Connor and Puria (2006) and while accounting for transmission delays across the tympanic membrane of approximately 25-40μs (O'Connor and Puria 2008; Dobrev et al. 2014).

5. Conclusion

This work demonstrated methodologies to quantify the full six degrees-of-freedom of the rigid body motion of the malleus-incus complex (MIC). The results indicate that under physiologically relevant levels of acoustical stimulation, the hinged rotational motion is dominant at frequencies below 1.5 kHz, but the motion of the malleus and incus becomes complex as other motion components increase their significance at higher frequencies. While the malleus and the incus behave like one rigid body with little relative motion below 1.5 kHz, the relative motion between the malleus and the incus gets larger at higher frequencies. The MIC attenuates the hinged rotational motion at frequencies above 2 kHz, and the incus has smaller rotational motion about the inferior-superior axis than the malleus above 2 kHz.

458 Future work, involving more samples, should include the quantification and analysis
459 of all motion components for the complete description of the behavior of the MIC under
460 physiologically relevant acoustic excitation and its effect on the middle-ear function.

References

Alian, W., Majdalawieh, O., Kiefte, M., Ejnell, H., Bance, M., 2013. The Effect of Increased Stiffness of the Incudostapedial Joint on the Transmission of Air-Conducted Sound by the Human Middle Ear. *Otology & Neurotology*, 34(8), 1503-1509.

Decraemer W.F., Khanna S.M., and Funnell W.R.J., 1994. A method for determining three-dimensional vibration in the ear. *Hear. Res.* 77(1-2), 19-37.

Decraemer W.F., Khanna S.M., and Funnell W.R.J., 1999. Vibrations at a fine grid of points on the cat tympanic membrane measured with a heterodyne interferometer. In EOS/SPIE International Symposia on Industrial Lasers and Inspection, Conference on Biomedical Laser and Metrology and Applications.

Decraemer W.F., de La Rochefoucauld O., Dong W., Khanna S.M., Dirckx J.J.J., and Olson E.S., 2007. Scala vestibuli pressure and three-dimensional stapes velocity measured in direct succession in gerbil. *JASA* 121, 2774–2791.

Decraemer, W., de La Rochefoucauld, O., Funnell, W., Olson, E.S., 2014. Three-Dimensional Vibration of the Malleus and Incus in the Living Gerbil, *JARO*, 15, 483-510.

Dobrev, I., Furlong, C., Cheng, J. T., Rosowski, J. J., 2014. Full-field transient vibrometry of the human tympanic membrane by local phase correlation and high-speed holography. *Journal of biomedical optics*,19(9), 096001-096001.

Ihrle, S., Eiber, A., Eberhard, P., 2015. Experimental investigation of the three dimensional vibration of a small lightweight object. *Journal of Sound and Vibration* 334: 108-119.

Gatto, M., Peeters, B., Coppotelli, G., 2010. Flexible shaker excitation signals for improved FRF estimation and non-linearity assessment. In Proceedings of the ISMA 2010 International Conference on Noise and Vibration Engineering.

Gerig, R., Ihrle, S., Röösli, C., Dalbert, A., Dobrev, I., Pfiffner, F., Eiber, A., Huber A.M., Sim J.H., 2015. Contribution of the incudo-malleolar joint to middle-ear sound transmission. Accepted in *Hear. Res.*

Goode, R. L., Killion, M., Nakamura, K., Nishihara, S., 1994. New knowledge about the function of the human middle ear: development of an improved analog model. *Otology & Neurotology*, *15*(2), 145-154.

Goode, R. L., Ball, G., Nishihara, S., & Nakamura, K., 1996. Laser Doppler Vibrometer (LDV) a new clinical tool for the otologist. *Otology & Neurotology*, *17*(6), 813-822.

Hato, N., Stenfelt, S., Goode, R.L., 2003. Three-dimensional stapes footplate motion in human temporal bones. *Audiology & Neuro-Otology,* 8, 140-152.

Huber, A. M., Schwab, C., Linder, T., Stoeckli, S. J., Ferrazzini, M., Dillier, N., Fisch, U., 2001. Evaluation of eardrum laser Doppler interferometry as a diagnostic tool. *The Laryngoscope*, 111(3), 501-507.

Huber, A. M., Ma, P., Felix, H., Linder, T., 2003. Stapes Prosthesis Attachment: The Effect of Crimping on Sound Transfer in Otosclerosis Surgery. *Laryngoscope*, 113, 853–858.

Kurokawa, H., Goode, R., 1995. Sound pressure gain produced by the human middle ear. *Am. J. Otology,* 113: 349-355.

Lauxmann, M., Eiber, A., Heckler, C., Ihrle, S., Chatzimichalis, M., Huber, A.M., Sim, J.H., 2012. In-plane motions of the stapes in human ears. *JASA*, 132(5), 3280-3291.

O'Connor, K. N., Puria, S., 2006. Middle ear cavity and ear canal pressure-driven stapes velocity responses in human cadaveric temporal bones. *JASA*, 120(3), 1517-1528.

O'Connor, K. N., Puria S., 2008. Middle-ear circuit model parameters based on a population of human ears. *JASA*, 123(1), 197.

Peacock, J., Dirckx, J., von Unge, M., 2015. Towards quantitative diagnosis of ossicular fixation: Measurement of stapes fixations using magnetically driven ossicles in human temporal bones. *Acta oto-laryngologica*, (0), 1-6.

Puria, S., 2003. Measurements of human middle ear forward and reverse acoustics: implications for otoacoustic emissions. *JASA*, 113(5): 2773-2789.

Puria, S., Sim, J. H., Shin M., Steele, C. R., 2007. A gear in the middle ear. *The 30th Association for Research in Otolaryngology Winter Research Meeting, Denver, Colorado*.

Puria, S., and Steele, C.R., 2010. Tympanic membrane and malleus-incus-complex co-adaptations for high-frequency hearing in mammals. *Hearing Research,* 263, 183-190.

Rosowski, J. J., Mehta, R.P., Merchant, S.N., 2004. Diagnostic utility of laser-doppler vibrometry in conductive hearing loss with normal tympanic membrane. *Otol. Neurotol.*, 25(3): 323–332.

Sim, J. H., Puria, S., Steele, C. R., 2004. Three-dimensional measurement and analysis of the isolated malleus-incus complex. In K. Gyo & H. Wada (Eds.), *The 3rd International Symposium on Middle Ear Mechanics in Research and Otology*, (pp. 61–67). Singapore: World Scientific.

Sim, J. H., Puria, S., 2008. Soft tissue morphometry of the malleus-incus complex from micro-CT imaging. *JARO,* 9: 5-21.

Sim, J. H., Puria, S., Steele, C.R., 2007. Calculation of the inertial properties of the malleus-incus complex from micro-CT imaging. *Journal of Mechanics of Materials and Structures*, 2 (8): 1515-1524.

Sim, J. H., Puria, S., 2009. An electro-magnetic force and moment motor: Application to small-scale biological structures. *IEEE Sensors Journal,* 9: 1924-1932.

Sim, J. H., Chatzimichalis, M., Lauxmann, M., Röösli, C., Eiber, A., Huber, A.M., 2010a. Complex stapes motions in human ears. *JARO*, 11(3): 329-341.

Sim, J. H., Chatzimichalis, M., Lauxmann, M., Röösli, C., Eiber, A., Huber, A.M., 2010b. Errors in measuring three-dimensional motions of the stapes using a laser Doppler vibrometer system. *Hear. Res.,* 270: 4-14.

Sim, J. H., Chatzimichalis, M., Röösli, C., Laske, R.D., and Huber, A.M., 2012. Objective assessment of stapedotomy surgery from round window motion measurement. *Ear & Hearing,* 33(5): 24-31.

Terdiman, P., 2001. Memory-optimized bounding-volume hierarchies. http://www.codercorner.com/Opcode.htm

Whittemore, K. R., Merchant, S. N., Poon, B. B., Rosowski, J. J., 2004. A normative study of tympanic membrane motion in humans using a laser Doppler vibrometer (LDV). *Hearing Research*, *187*(1), 85-104.

Willi, U. B., Ferrazzini, M. A., Huber, A. M., 2002. The incudo-malleolar joint and sound transmission losses. *Hearing research*, *174*(1), 32-44.

Figure Captions

Fig 1. Schematic illustration of the measurement setup.

Fig 2. 3-D features of the middle-ear ossicles and the markers aligned into the LDV measurement frame (a) and illustration of the ray-tracing with virtual laser beams for identification of the *Z* coordinates of the measurement points (b), for the orientation of TB1.

Fig 3. Measurement points in the three LDV measurement frames with three different orientations (a-c) and all the corresponding points registered in the intrinsic frame (d), for TB1.

Fig 4. Validation of calculation of rigid body motion (RBM) components.

Fig 5. Rigid body motion (RBM) components of the malleus (solid) and the incus (dashed), normalized by the ear canal pressure, (a) for fresh temporal bone (TB1) and (b) for frozen temporal bone (TB2).

Fig 6. Velocities at the umbo of the malleus and at the lenticular process of the incus (LPI), normalized by the ear canal pressure, (a) for fresh temporal bone (TB1) and (b) for frozen temporal bone (TB2). The shaded areas, outlined with dashed lines, in the figures indicate the normal ranges (95% confidence interval) of the umbo motion (light gray), based on literature, and the stapes motion (dark gray), based on ASTM standard.

Fig 7. Magnitudes of the measured data (solid) in comparison with the magnitude of the corresponding components recalculated from the obtained RMB (dashed), for the measurement points on the incus in the TB2.

Fig 8. Ratios of the velocity at the lenticular process of the incus (LPI) to the velocity at the umbo for the component in the z direction (lateral-medial direction).

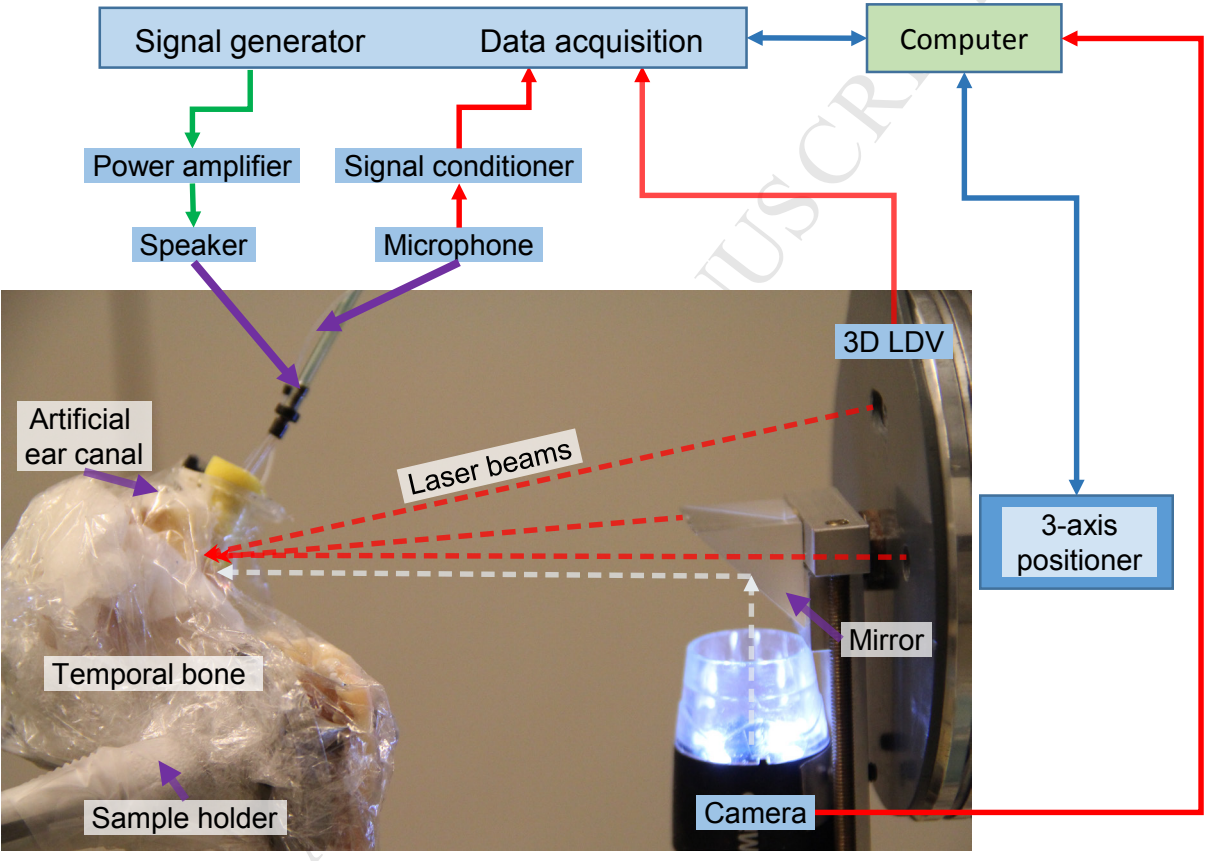
Signal generator
Data acquisition
Computer
Power amplifier
Signal conditioner
Speaker
Microphone
3D LDV
Artificial ear canal
Laser beams
3-axis positioner
Mirror
Temporal bone
Sample holder
Camera

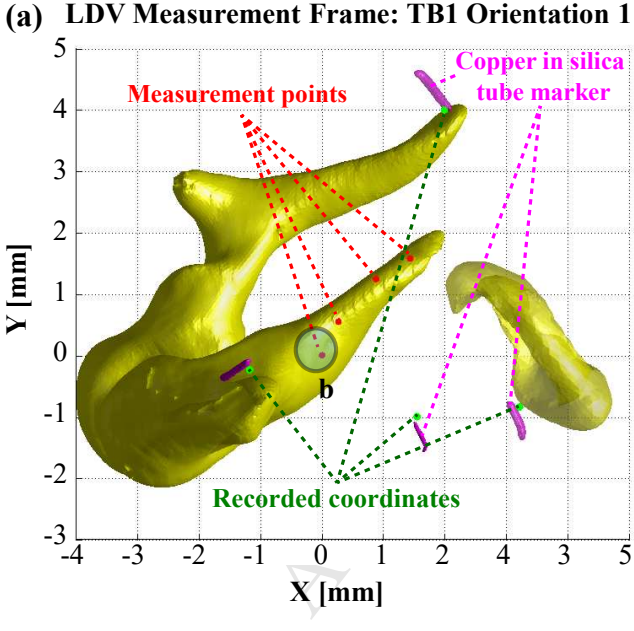

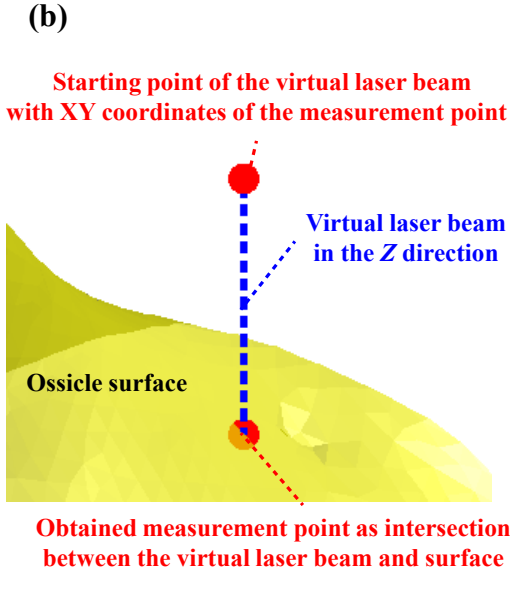

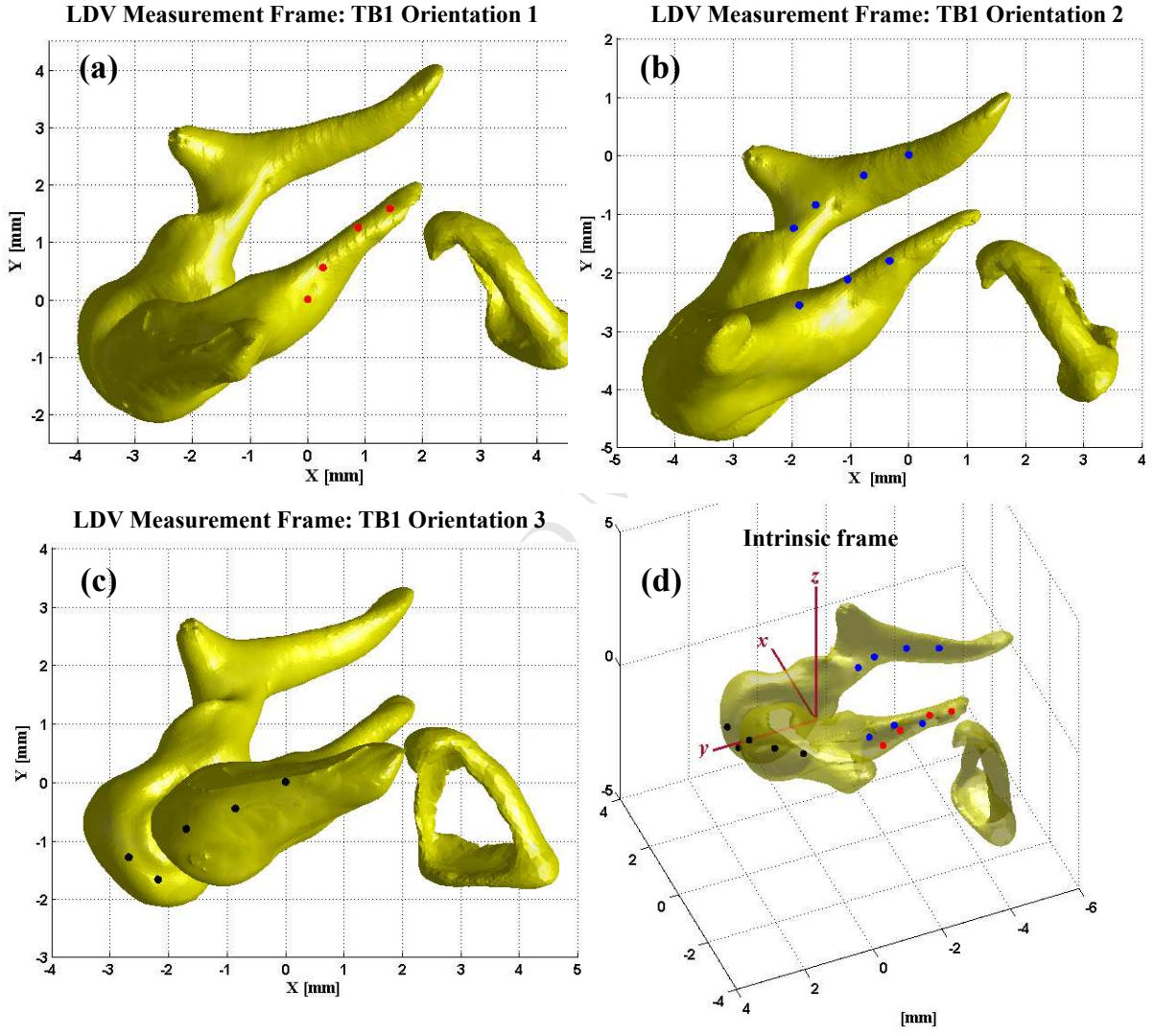
LDV Measurement Frame: TB1 Orientation 1
(a)
Y [mm]
X [mm]
LDV Measurement Frame: TB1 Orientation 2
(b)
Y [mm]
X [mm]
LDV Measurement Frame: TB1 Orientation 3
(c)
Y [mm]
X [mm]
Intrinsic frame
(d)
z
x
y
[mm]

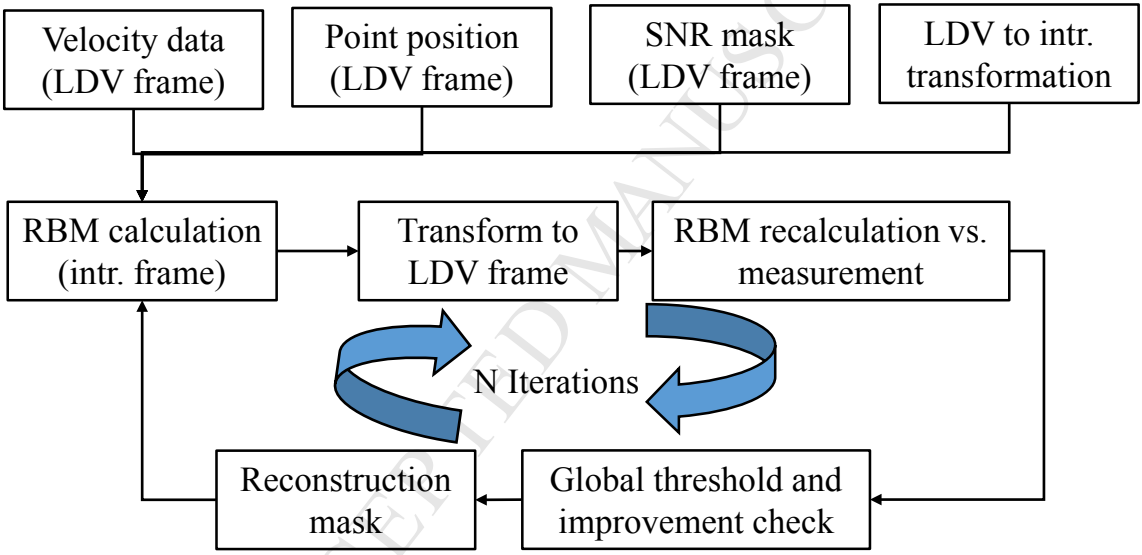

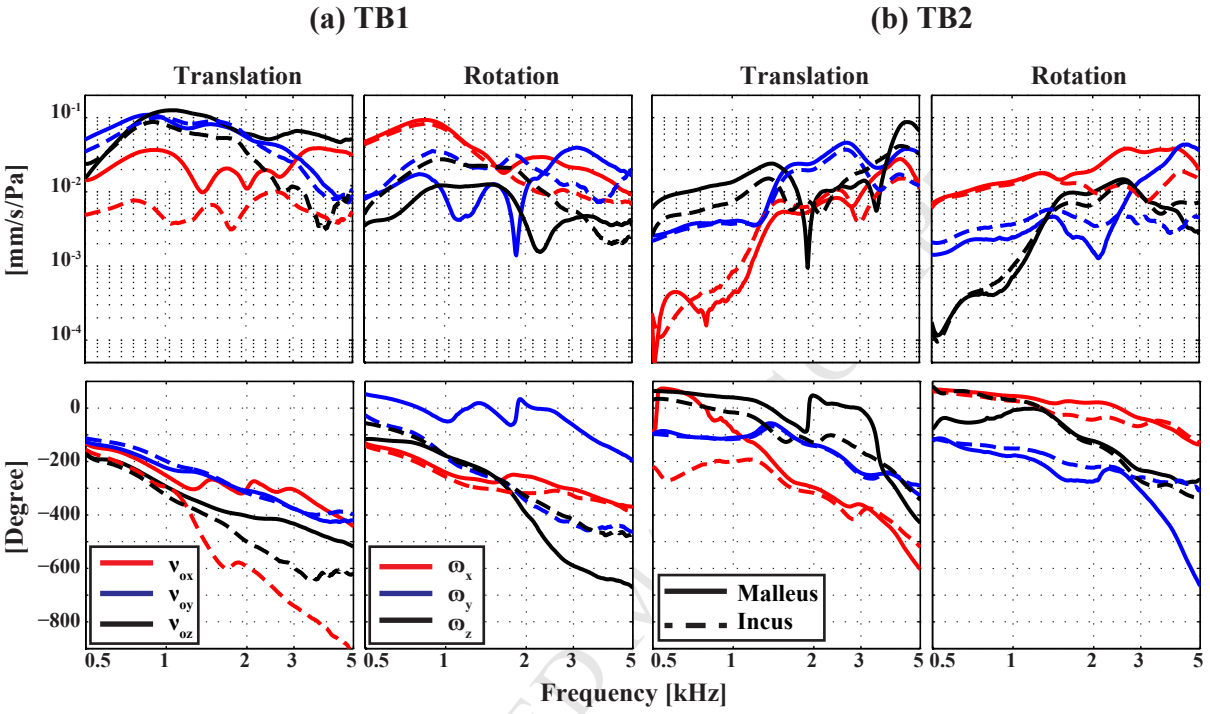

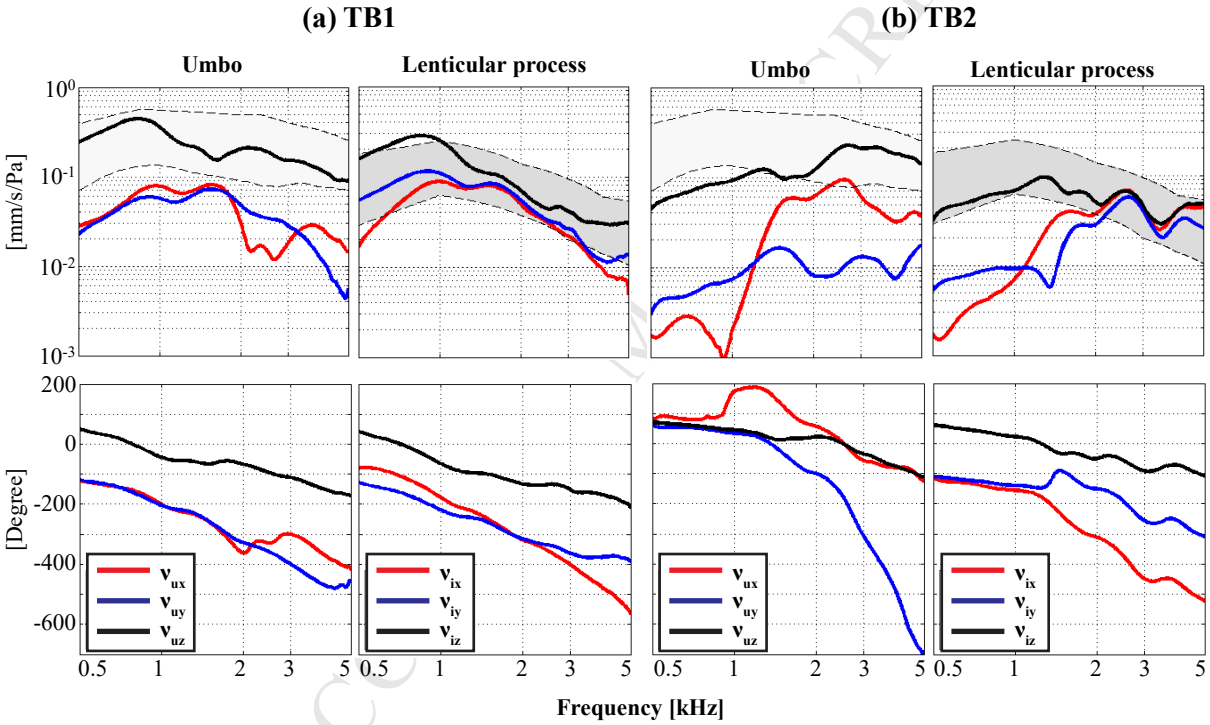

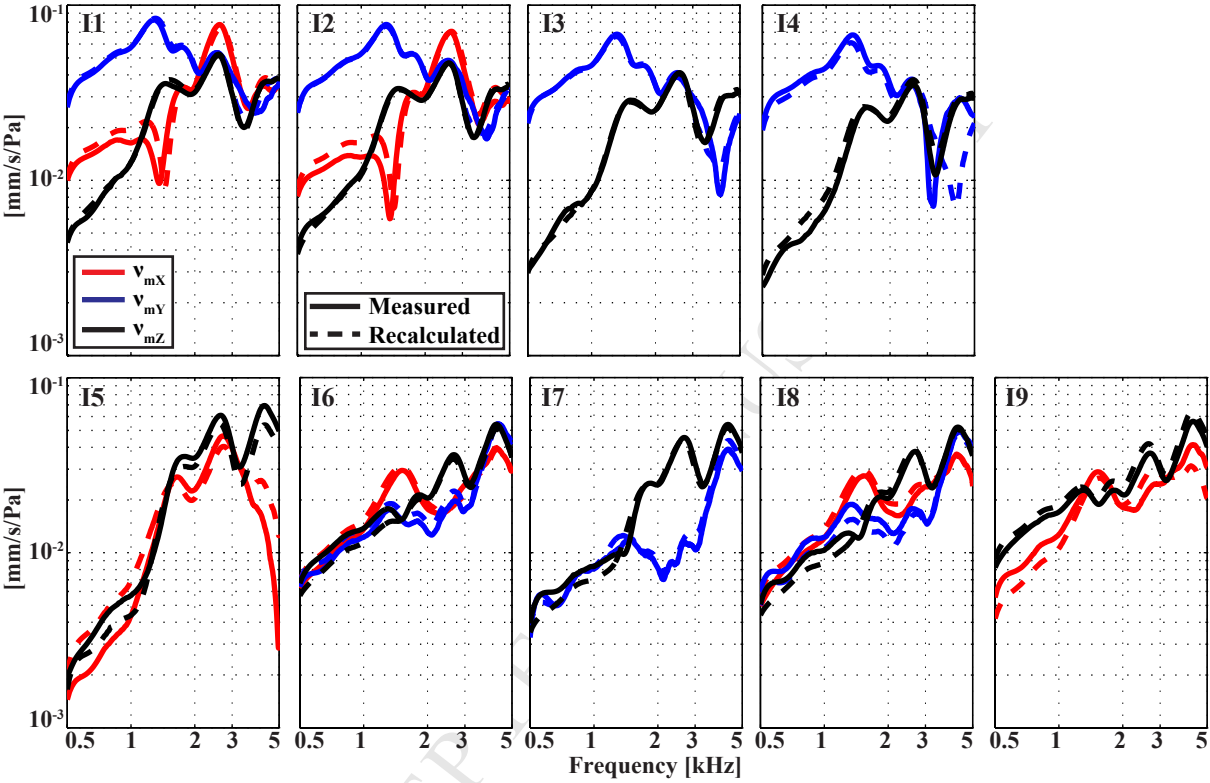

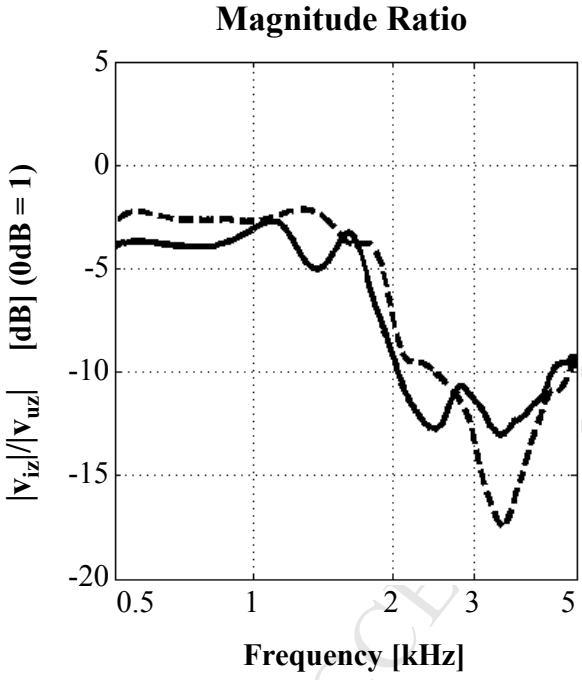
Magnitude Ratio
$|V_{iz}|/|V_{uz}|$ [dB] (0dB = 1)
5
0
-5
-10
-15
-20
0.5
1
2
3
5
Frequency [kHz]

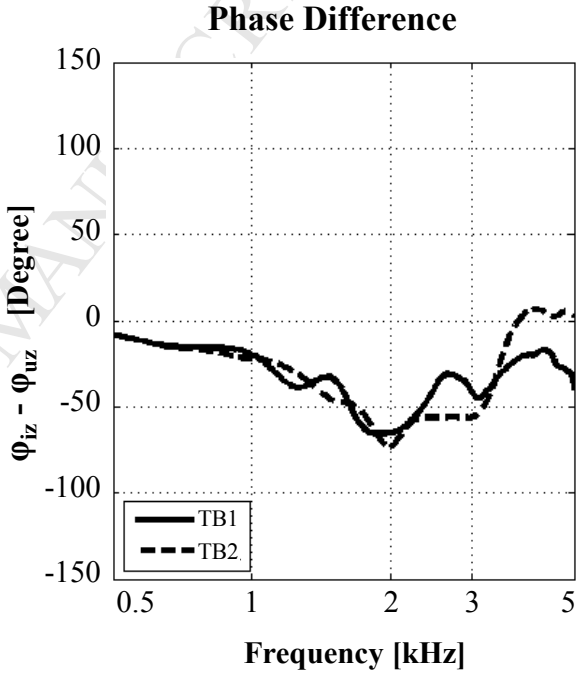
Phase Difference
$\varphi_{iz} - \varphi_{uz}$ [Degree]
150
100
50
0
-50
-100
-150
TB1
TB2
0.5
1
2
3
5
Frequency [kHz]

Research Highlights

- Demonstrated methodologies to quantify the full six degrees-of-freedom of the rigid body motion of the malleus-incus complex (MIC).
- The MIC motion is defined by a predominant hinged rotational component below 1.5 kHz.
- The rotation about the inferior-superior direction, or “twisting motion”, in the malleus has larger magnitudes than the corresponding component in the incus above 3 kHz.
- While the magnitude of the transfer function of the MIC decreases with frequency, its spatio-temporal complexity increases significantly